PIV Studies on the Effect of the Number of Lobes in a Supersonic ESTS Lobed Nozzle

S. K. Karthick, V. Albin, Srisha M. V. Rao, and Gopalan Jagadeesh

Abstract ESTS lobed nozzle is found to be efficient in supersonic jet mixing applications. In this study, the influence of a number of lobes on the aspects of mixing is probed using the 2D-PIV measurements. From the analysis of the obtained 2D velocity field, the kinematics of the lobed nozzle is reported for the first time experimentally. Centerline velocity decay, turbulence intensity, and mass efflux are calculated to compare the influence of a different number of lobes in the lobed nozzle. The conical nozzle is used as the base nozzle for comparison. It is observed that the three-lobed nozzle is efficient in terms of mixing and jet spread. Especially an increment of 70% in the jet spread is observed for three-lobed nozzle. The primary reason for the observed enhancement is due to the higher penetration of the lobe tip into the core flow (by 30% compared with the six-lobed nozzle) which produces larger-scale streamwise vortices than the other cases under consideration.

1 Introduction

Exotic nozzle geometries are found to be an effective passive technique to enhance mixing and entrainment in supersonic jets [1, 2]. They are found to be useful in the design and development of high-performance supersonic ejectors and combustors. Recently, supersonic Elliptic Sharp Tipped Shallow (ESTS) lobed nozzles are found to be efficient in mixing enhancement [3, 4]. These nozzles are easy to produce, and the shallow tips are found to be effective in enhancing the mixing process by producing streamwise vortices with lower total pressure loss. Typical time-averaged flow field observed in the conical nozzle and the four-lobed ESTS nozzle using planar laser Mie scattering (PLMS) imaging is shown in Fig. 1. Key features like free shear layer, weak shocks, and higher jet spread can be easily observed in four-lobed ESTS nozzle (Fig. 1b). However, the sufficient number of lobes required for the optimized geometry of a supersonic ESTS lobed nozzle is still unclear

S. K. Karthick (✉) · V. Albin · S. M. V. Rao · G. Jagadeesh
Department of Aerospace Engineering, Indian Institute of Science, Bangalore, India
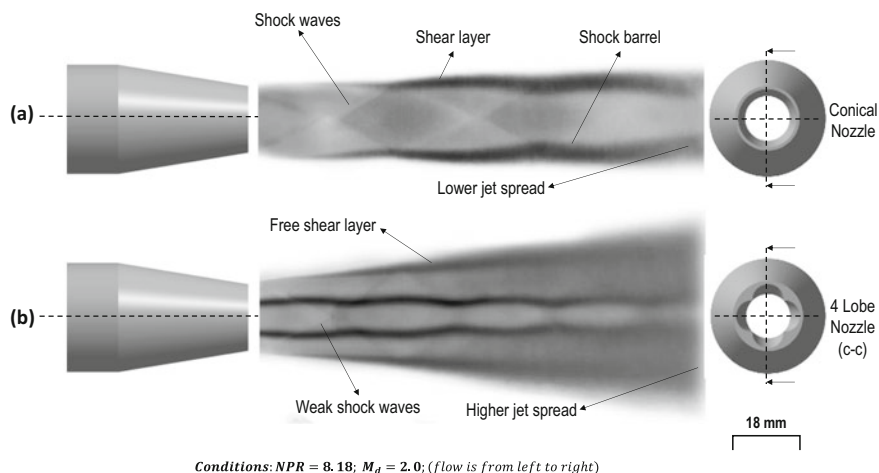
Fig. 1 Time-averaged planar laser Mie scattering (PLMS) image taken along the flow direction for (**a**) Conical nozzle and (**b**) Four-lobed ESTS nozzle (crest-crest, c-c) shows the distinct flow features, especially jet spread, in the case of petal nozzle compared with conical nozzle (conditions: NPR = 8.18; M_d = 2.0; flow is from left to right)

which motivates the authors to study further. Fluid mixing and entrainment can be better understood through the momentum exchange happening between the nearby fluids. The variations going on in the momentum flux of the jet could be easily studied by monitoring the kinematic properties of the moving fluid both spatially and temporally. Two-dimensional planar image velocimetry (2D-PIV) technique is chosen to understand the supersonic free jet flow field from the ESTS and conical nozzle, as it is a nonintrusive optical flow diagnosis to measure the flow velocity at a better spatial resolution.

2   Experiments

Experiments are carried out in the supersonic blowdown facility in LHSR, IISc – Bangalore. Nozzles are mounted at the end of the stagnation chamber. In the case of lobed nozzles, the positions are varied by rotating the nozzle and clamping it using the grub screw. More details regarding the rigging and sizing of the facility can be found in the work of Rao [3].

2.1   2D-PIV Technique

Currently employed 2D-PIV system comprises a Nd:YLF dual-cavity Litron laser (527 nm), operating at 0.8–1.0 kHz repetition (each cavity), with a pulse separation (dt) of 0.7 μs and with a maximum energy of 24 mJ/pulse. Consistent pulse segregation in the double-pulse operation mode of the laser is ensured by using the Laser Time Stabilizer Unit from LaVision. The primary supersonic flow field is seeded using the refined sunflower oil particles in the beginning portion of the stagnation chamber itself. The oil particles are generated using the in-house particle seeder [5] that works on the principle of modified Laskin nozzle. The ambient is seeded with smoke particles so that the entrained flow into the shear layer of the supersonic jet can be captured clearly. The particle size varies between 0.6 and 1.2 μm and provides a response time of 0.8–3.0 μs in the shock-laden flow field. A Phantom Miro 110 camera is used in the frame-straddling mode at full-frame resolution of 1280 × 800 pixels (20 μm pixel width). From the nozzle exit, 12D along the flow direction and 3D along the transverse flow direction are selected as the field of view. The nozzle exit is kept in the middle-left edge of the frame which gives an effective spatial resolution of 0.17 mm/pixel. A 527 nm band-pass filter is used to avoid parasite reflections and stray light from the background. A Nikon AF-S DX Micro 40 mm prime lens is used at f/2.8 to capture the scattering light better in the camera. The laser beam is transported to the required location using the guide arm, and a thin sheet of the laser (<1 mm thick) is formed using the appropriate sheet optics. The laser system and the camera are synced and controlled by the high-speed control (HSC) unit. DaVis 8.4 module is used as the software interface during the operation. Planar velocity fields are computed using the adaptive cross-correlation algorithm with a multi-pass (three times) decreasing window size from 64 × 64 pixels to 32 × 32 pixels. Nearly 800 images are used to represent the time-averaged velocity field, and the uncertainty involved in the velocity field computations is found to be not more than ±15 m/s. A typical schematic of the experimental facility for 2D-PIV studies can be seen in Fig. 2a.

2.2   Flow Conditions

For the cases discussed in this paper, three different numbers of lobes (3, 4, and 6) are considered, and they are compared with the base nozzle that is conical. The key dimensions of the nozzles can be seen in Fig. 2b, c. The nozzle is operated at three different conditions as shown in Table 1. The nozzles are operated for almost 3 s during which the PIV images are acquired. The instantaneous velocity field is represented as $V = \overline{V} + V'$, and the components of the given velocity vector can be represented as $V = u + v$ throughout this paper.

Fig. 2 (**a**) Typical schematic of the experimental facility for 2D-PIV studies in supersonic nozzle flows; (**b**) Cross section of the conical nozzle; (**c**) Cross section of the four-lobed nozzle. Key dimensions of the nozzle are marked in the figure itself
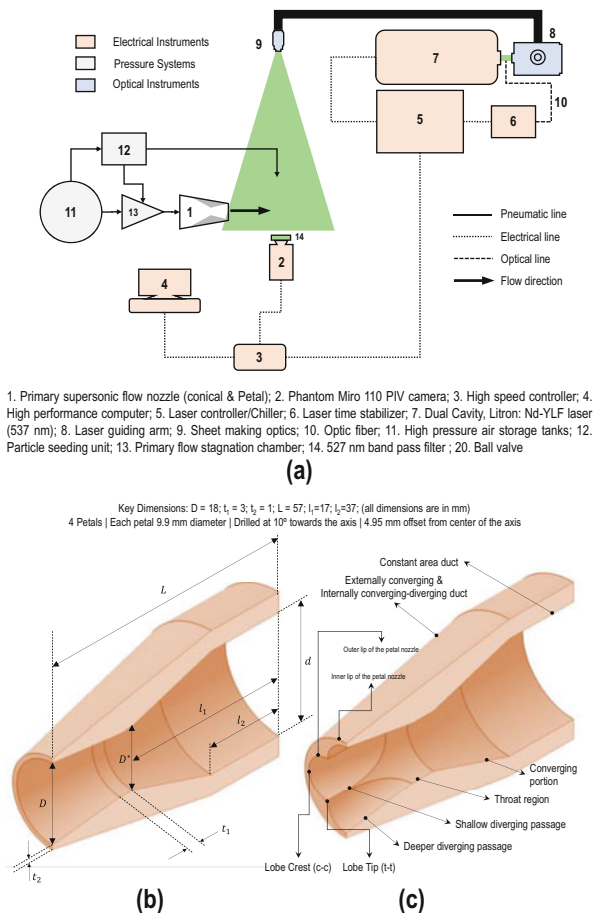

1. Primary supersonic flow nozzle (conical & Petal); 2. Phantom Miro 110 PIV camera; 3. High speed controller; 4. High performance computer; 5. Laser controller/Chiller; 6. Laser time stabilizer; 7. Dual Cavity, Litron: Nd-YLF laser (537 nm); 8. Laser guiding arm; 9. Sheet making optics; 10. Optic fiber; 11. High pressure air storage tanks; 12. Particle seeding unit; 13. Primary flow stagnation chamber; 14. 527 nm band pass filter ; 20. Ball valve

(a)

Key Dimensions: D = 18; t_1 = 3; t_2 = 1; L = 57; l_1=17; l_2=37; (all dimensions are in mm)
4 Petals | Each petal 9.9 mm diameter | Drilled at 10° towards the axis | 4.95 mm offset from center of the axis

(b) **(c)**

Table 1 Experimental conditions observed in the nozzle flow studies

M_d	P_o (bar)	NPR	M_j	Nozzle operating condition
2.0	3.54	4.01	1.56	Overexpanded (OE)
	6.52	7.61	1.99	Nearly expanded (NE)
	7.20	8.18	2.03	Slightly under-expanded (UE)

M_d nozzle design Mach number, M_j fully expanded jet Mach number, P_o total pressure of the primary flow, P_a ambient pressure, 0.88 bar, NPR nozzle pressure ratio, P_0/P_a, T_0 total temperature, 300 K

3 Results and Discussions

Most of the discussions will be on the nozzle flows at NPR = 4.01 for brevity. Typical 2D velocity field obtained for different nozzles and at different operating conditions is shown in Fig. 3. From Fig. 3a, it can be seen that the spreading rate is
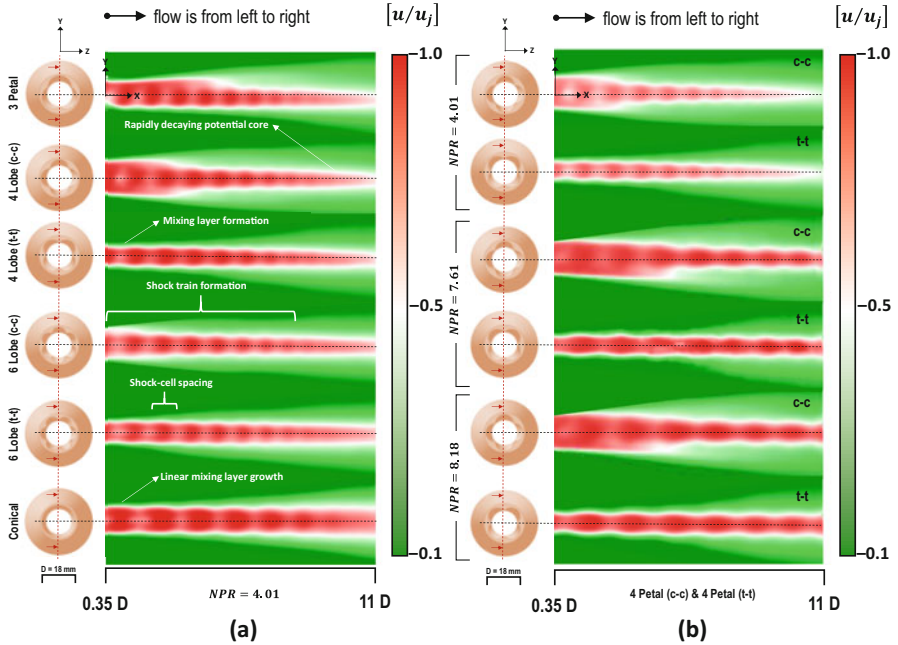
Fig. 3 Time-averaged, normalized 2D velocity field observed for $M_d = 2.0$ nozzle flows; (**a**) Different numbers of lobes in the lobed nozzles and conical nozzle at NPR = 4.01; (**b**) Different NPR in the case of four-lobed nozzle at two cross-sectional planes (crest-crest, c-c, and tip-tip, t-t)

maximum for three-lobed nozzle. Also, from Fig. 3b, it can be seen that the influence of NPR on the jet spread is not significant for the four-lobed nozzle; however, the length of the potential core is affected. The penetration of the lobe tip might be one reason for this behavior.

3.1 Centerline Velocity Decay

In Fig. 4, normalized centerline velocity decay is shown for all the nozzles at NPR = 4.01. From the figure, it is evident that velocity is decaying at a faster rate for the three-lobed nozzle compared with the other cases. On the contrary, the shock strength in the potential core shows a different trend. The peaks and valleys in the near field of the jet (<5D) shed information regarding the shock strength. Analyzing the magnitude between peaks and valleys for all the cases, six-lobed nozzle is found to have a potential core with lower shock strength compared with other cases. However, the shock cell spacing is comparative in the lobed nozzle than in the conical nozzle. As told earlier, for a similar exit area, the penetration of lobe tip in the case of three-lobed nozzle is larger than the six-lobed nozzle (by 30%).
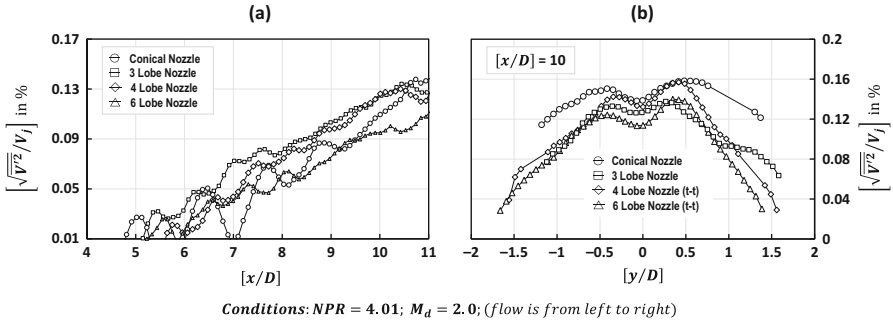
Fig. 4 (**a**) Turbulent intensity variation along the centerline for different lobed nozzles and conical nozzle; (**b**) Turbulent intensity variation along the transverse section (x/D = 10) for different lobed nozzles and conical nozzle (conditions: NPR = 4.01; M_d = 2.0; flow is from left to right)
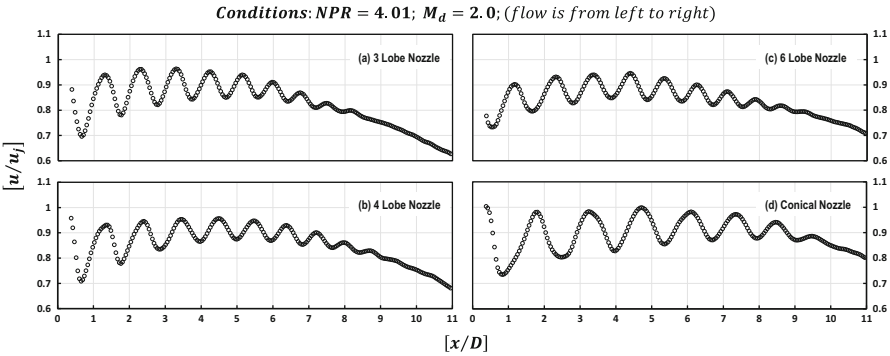

Fig. 5 Normalized centerline velocity decay observed in different nozzles; (**a**) Three-lobed nozzle; (**b**) Four-lobed nozzle; (**c**) Six-lobed nozzle; (**d**) conical nozzle (conditions: NPR = 4.01; M_d = 2.0; flow is from left to right)

3.2 Turbulent Intensity (TI)

Turbulent intensity (TI) variations along the centerline and the transverse sections provide information regarding the mixing aspects and jet spreading. In Fig. 5a, the centerline TI variations for different nozzles are plotted. Along the jet direction, due to the interaction of the inner shear layer with the potential core and the turbulence production due to the shocks, TI increases. Due to higher shock strength in the conical nozzle, the TI fluctuates between 1% and 5% till 8D and gradually increases to 11% at 11D. However, in the case of three-lobed nozzle, the increment in TI is observed from 6D onward and reaches to a maximum of 14% at 11D. This again justifies the argument made in Sect. 3.1. Figure 5b yields information regarding the jet spread at [x/D] = 10. There is a prominent asymmetry in the jet spread (almost by 70%) from the axis line for three-lobed nozzle owing to its asymmetry on the lobe placement in the considered cross section. Except for conical nozzle, lobed nozzles have a comparable jet spread.
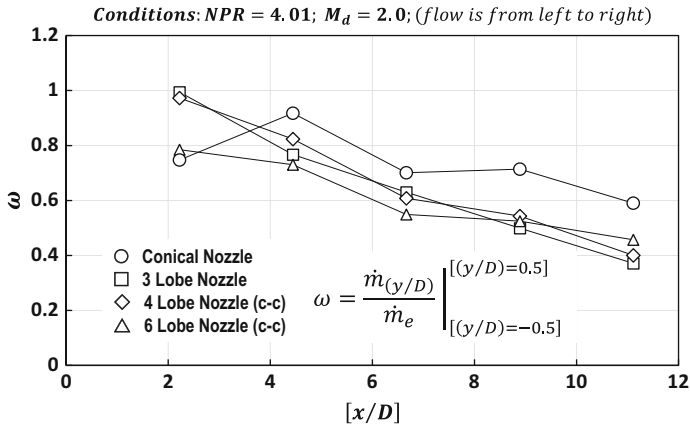
Fig. 6 Variation of mass flux inside the imaginary tube of 1D diameter for different lobed nozzles and conical nozzles. The representation is aimed to qualitatively figure out the effect of the number of lobes through the mass transfer on the jet spread and fluid mixing (conditions: NPR = 4.01; M_d = 2.0; flow is from left to right)

3.3 Mass Efflux

To comment on the momentum transferred from the primary flow to the entrained ambient flow for different lobed nozzles, an imaginary tube of diameter 1D is considered, and the ratio of the mass flow rate (ω) is calculated at five different sections. Irrespective of the radial velocity profile obtained for different nozzles, the analysis is carried out to emphasize the influence of lobe numbers qualitatively. From Fig. 6, in the near field, due to higher shock strength, there will be a mass deficient in conical nozzle flows and hence the fluctuations in the trend. But considering the values downstream, it can be seen that the lobed nozzles are effective in transferring the momentum to the entrained secondary fluid. In the considered experiments, the three-lobed nozzle loses ω rapidly by 40% than the conical nozzle. Also, the six-lobed nozzle is observed to lose ω by only 25%. It once again confirms the influence of the lobe tip penetration on the jet spread and mixing. The penetration of the lobe tip plays a prominent role as it dictates the strength of the generated streamwise vortices.

4 Conclusions

Experiments are carried out for a different number of lobes in the ESTS lobed nozzle, and they are compared with the conical nozzle. 2D-PIV measurements are carried out, and the velocity field is used to compare the kinematics of the considered nozzles. Three-lobed nozzle shows better mixing and spreading characteristics

owing to the higher penetration length of the lobe tip than the other nozzle. Further studies in terms of the streamwise vorticity generation and different operating conditions are underway.

References

1. T.G. Tillman et al., J. Propuls. Power **8**, 2 (1992)
2. K.B.M.Q. Zaman, J. Fluid Mech. **383**, 197–228 (1999)
3. S.M.V. Rao, G. Jagadeesh, Appl. Therm. Eng. **71**, 1 (2014)
4. S.M.V. Rao et al., Appl. Therm. Eng. **99**, 599 (2016)
5. S.K. Karthick et al., J. Indian Inst. Sci. **96**, 1 (2016)